MATHEMATICAL MODELING AND COMPUTING, Vol. 10, No. 4, pp. 1269–1280 (2023)

Haar wavelet collocation method for solving stagnation point over a nonlinearly stretching/shrinking sheet in a hybrid nanofluid with slip effect

Hasanah N. S.[1], Rasedee A. F. N.[2], Bachok N.[1], Wong T. J.[3], Hasan M.[4,*]

[1] *Department of Mathematics and Statistics, Faculty of Science, University Putra Malaysia, 43400 Serdang, Selangor, Malaysia*
[2] *Faculty of Economics and Muamalat, University Sains Islam Malaysia, Malaysia*
[3] *Department of Basic Sciences and Engineering, Faculty of Agriculture and Food Science, University Putra Malaysia, Bintulu Campus, Nyabau Road, Bintulu, Sarawak, 97008, Malaysia*
[4] *Centre of Foundation Studies for Agricultural Science, University Putra Malaysia*
[*] *Corresponding author: mohdhasan@upm.edu.my*

(Received 26 September 2023; Revised 18 November 2023; Accepted 19 November 2023)

The study of stagnation point flow and heat transfer over a stretching/shrinking sheet in a hybrid nanofluid has potential applications in a variety of fields. In order to investigate the properties of fluid flow and heat transfer, this study must solve the governing mathematical model(partial differential equations). By utilizing similarity variables, the model is transformed into a system of ordinary differential equations. The study employs a novel numerical scheme that combines the power of Haar wavelets with the collocation method to solve these ordinary differential equations. Through this approach, the study can predict several important values related to the fluid's flow and heat transfer, including the skin friction coefficient, local Nusselt number, and the profiles of velocity, temperature which can be influenced by the governing parameters of the model.

Keywords: *hybrid nanofluids; nonlinearly stretching/shrinking; stagnation point; Haar wavelet.*

2010 MSC: 35Q35, 35Q79, 76A02, 76D05 **DOI:** 10.23939/mmc2023.04.1269

1. Introduction

Highly efficient heat transfer technologies are crucial for various industrial applications, especially in processes involving cooling or heating. However, classical heat transfer fluids such as oil, water, and ethylene glycol have poor thermal conductivity, which limits their performance. To address this issue, Choi and Eastman [1] developed a novel fluid called "nanofluid" by incorporating nanosized solid particles with high thermal conductivity into the classical fluids [2,3]. Nanofluid offers superior thermophysical attributes when compared to traditional fluids, resulting in improved heat transfer capabilities. Interestingly, even a small number of nanoparticles can significantly increase thermal conductivity [4]. Suresh et al. [5,6] undertook experimental investigations to augment the thermal conductivity of base fluids. Their findings unveiled the potential of hybrid nanofluids, which are a mixture of two different nanoparticles dispersed in a base fluid, to amplify the principle fluid's heat capacity. For instance, metallic nanoparticles such as zinc, copper, and aluminium boast remarkable thermal conductivities, while aluminium oxide demonstrates superior chemical inertness and stability. According to scientific studies, hybrid nanofluid have the potential to supplant mono nanofluid, particularly in the automotive, refrigeration systems, photovoltaic modules, electromechanical, industrial processes, and solar energy applications [7–9]. Numerous researchers have focused on studying the heat transfer characteristics of hybrid nanofluids in light of their potential applications. Devi [10] were pioneers in this field, con-

This work was supported by Research Grant Putra, University Putra Malaysia.

ducting the first to numerically investigate a stretching surface using boundary layer theory in hybrid nanofluids with Newtonian heating. Additionally, Hayat and Nadeem [11] made an intriguing discovery that hybrid nanofluids had a faster cooling rate than nanofluids due to radiative heat generation and chemical reactions. Furthermore, recent work by Anuar et al. [12] explored the flow of hybrid nanofluid due to stagnation point flow on a stretch/shrink surface.

Stagnation-point flow, a phenomenon occurring in the stagnation area of a solid surface at the front of a blunt-nosed body, can manifest whether the body is stationary or moving through the fluid. The area around the stagnation point has the greatest pressure and heat transfer rates, as well as the highest mass deposition rates. Consequently, researchers have taken a keen interest in scrutinizing stagnation point flow that flows past a surface that is either stretching or shrinking. References [13–15] explored the magnetohydrodynamic (MHD) flow and heat transfer that is influenced by a stretching/shrinking surface is quite important in extrusion processes such as metal sheet extrusion, polymer extrusion, and various manufacturing procedures like glass blowing and plastic film drawing.

Numerous difficulties arise in solving nonlinear ordinary differential equations over an infinite interval by using numerical and semi-numerical techniques discussed by many researchers. Established numerical methods such as Shooting method, Keller box method, and Finite element method (FEM) and these techniques require good initial guesses when tackling the solution to boundary value problems (BVPs) at numerous values of the significant parameters. Although the shooting method is effective for straightforward problems, such as the projectile problem, its effectiveness relies on the stability of the initial value problem that must be solved at each iteration. Unfortunately, for numerous stable boundary value problems, the corresponding initial value problems (from either endpoint to the other) are insufficiently stable for shooting to succeed. Consequently, the shooting methods may not always be computationally suitable for the whole range of practical boundary value problems, especially those occurring over extended or infinite interval. Hence, shooting offers limited applicability in addressing some practical engineering problems [16,17]. Semi-analytical methods depend on the presence of small perturbation parameters and initial base functions, but they encounter divergence issues when the boundary-layer variable tends to infinity. To address this, semi-analytical methods frequently turn to Pade approximations as a means to enhance the radius of convergence. Because these methods have convergence difficulties and mandatory prerequisites, it is crucial to explore and develop novel, efficient techniques that can overcome all obstacles. Presently, wavelet methods are gaining momentum as a promising alternative to traditional numerical and semi-analytical methods Karkera et al. [18].

In recent decades, wavelet methods have gained significant attention in numerical analysis as an alternative to conventional approaches. Distinguished researchers like Meyer, Morlet, Grossmann, Daubechies [19], and others explored the mathematical properties of wavelet functions in the late 20th century. Various types of wavelets have been utilized to tackle differential equations, with particular emphasis on the Haar wavelet method, which has gained significant consideration due to its numerous advantages. Alfred Haar's pioneering work in 1910 introduced the Haar wavelet, and subsequent advancements were made by Chen and Hsiao [20], who derived the operational matrices for Haar wavelets. Lepik [21] further extended this methodology, providing a systematic approach for solving differential equations on grids with uniform spacing. Recent works have unveiled the potential of Haar wavelets in solving integral and delay differential equations [22, 23] and as well as establishing the error analysis in the Holder classes [24]. Moreover, innovative combinations of the Haar wavelet method with the quasi-linearization technique [25] have been employed by Arifeen et al. [26] and Jiwari et al. [27] for the approximate solutions for nonlinear ordinary differential equations and partial differential equations. However, while most of the research has concentrated on the problem of finite domains, limited research has been done to study boundary value problems with infinite domains using Haar wavelets [18]. Based on the published literature, this study delves into the examination of flow properties and heat transfer of a hybrid nanofluid over a stretching/shrinking sheet within the context of stagnation point flow in infinite domain.

2. Haar wavelets

The Haar wavelet is a square-shaped wave with a magnitude of ± 1 at certain intervals and zero elsewhere that forms a variety of wavelet families or basis. The Haar wavelet is classified as compact, dyadic, discrete, and orthonormal. It consists of pairs of piecewise constant functions and it is the numerically simplest of all wavelet families. The one-dimensional Haar wavelet family for $x \in [0, 1)$ is defined as

$$h_i(x) = \begin{cases} 1, & \text{for } x \in [\alpha, \beta), \\ -1, & \text{for } x \in [\beta, \gamma), \\ 0, & \text{elsewhere,} \end{cases}$$

where $\alpha = \frac{k}{m}$, $\beta = \frac{k+0.5}{m}$, $\gamma = \frac{k+1}{m}$. $h_1(x)$ is the scaling function for the family can be defined as

$$h_1(x) = \begin{cases} 1, & \text{for } x \in [0, 1), \\ 0 & \text{elsewhere.} \end{cases}$$

The Haar series is constructed by taking linear combinations of the scaled and translated Haar wavelet functions. These combinations are weighted by the coefficients that depend on the properties original function. Haar wavelet integration also can be expanded into Haar series. One significant advantage of the Haar wavelet is the ability to integrate it analytically at arbitrary times. By referring to Karkera et al. [18], these integrals can be determined as follows:

$$\begin{aligned} p_{i,1}(t) &= \int_0^x h_i(t)\, dt \\ &= \begin{cases} x - \alpha, & \text{for } x \in [\alpha, \beta), \\ \gamma - x, & \text{for } x \in [\beta, \gamma), \\ 0, & \text{elsewhere,} \end{cases} \end{aligned}$$

$$\begin{aligned} p_{i,2}(t) &= \int_0^x p_{i,1}(t)\, dt \\ &= \begin{cases} \frac{1}{2}(x - \alpha)^2, & \text{for } x \in [\alpha, \beta), \\ \frac{1}{4m^2} - \frac{1}{2}(\gamma - x)^2, & \text{for } x \in [\beta, \gamma), \\ \frac{1}{4m^2}, & \text{for } x \in [\gamma, 1), \\ 0, & \text{elsewhere.} \end{cases} \end{aligned}$$

Likewise, $P_{l+1,i}(t) = \int_0^t P_{l,i}(x)\, dx$, $l = 2, 3, \ldots$.

3. Mathematical formulation

A steady boundary layer of a hybrid's nanofluid for solving stagnation point flow over a nonlinearly stretching/shrinking sheet with slip effect by Haar wavelet was studied numerically. Figure 1 shows the schematic illustration of the boundary layer problem where the x-axis is considered along the shrinking sheet in the vertical direction while the y-axis is perpendicular to it. Then, the surface is supposed to stretch/shrink with the velocity $U_w(x) = ax^n$, where $a > 0$ indicates constant flow and the presence of slip effect condition $u = U_w(x) + L(\frac{\partial u}{\partial y})$, given that $L = L_1 x^{-(\frac{n-1}{2})}$ is the slip factor. Meanwhile for $U_\infty(x) = bx^n$ is the external (inviscid) fluid's velocity with $b > 0$ as the stagnation-point's strength. The surface is maintained at constant temperature T_w and the temperature of ambient T_∞.

As a consequence of the previously mentioned boundary layer assumptions, the equations of continuity, momentum, and energy are formulated by Bachok et al. [28] and Anuar et al. [29],

$$\frac{\partial u}{\partial x} + \frac{\partial v}{\partial y} = 0, \tag{1}$$

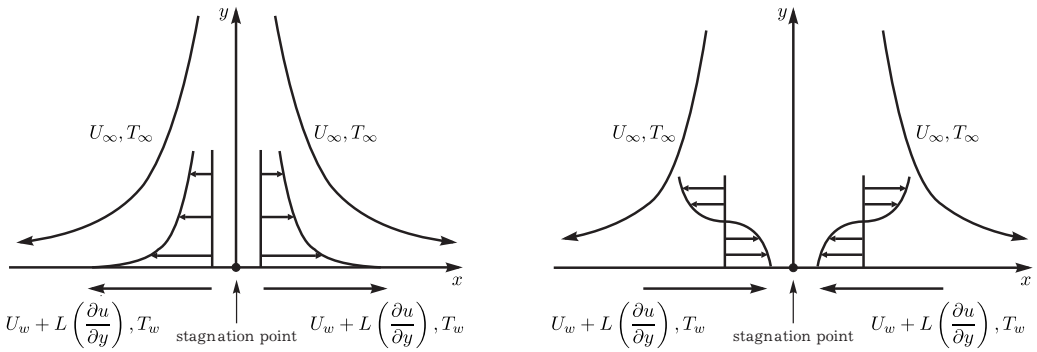

Fig. 1. Schematic illustration of the flow.

$$u\frac{\partial u}{\partial x} + v\frac{\partial u}{\partial y} = U_\infty \frac{dU_\infty}{dx} + \frac{\mu_{hnf}}{\rho_{hnf}}\frac{\partial^2 u}{\partial y^2}, \tag{2}$$

$$u\frac{\partial T}{\partial x} + v\frac{\partial T}{\partial y} = \alpha_{hnf}\frac{\partial^2 T}{\partial y^2} \tag{3}$$

along with the boundary conditions

$$\begin{aligned} &v = 0, \quad u = U_w(x) + L\left(\frac{\partial u}{\partial y}\right), \quad T = T_w \ \text{ at } \ y = 0, \\ &u \to U_\infty(x), \quad T \to T_\infty \ \text{ as } \ y \to \infty. \end{aligned} \tag{4}$$

Then, the correlation of the physical properties is shown in Table 1 [30–32].

Table 1. Hybrid nanofluid thermophysical properties.

Properties	Hybrid Nanofluid Correlations
Thermal Diffusivity	$\alpha_{hnf} = \frac{k_{hnf}}{(\rho C_p)_{hnf}}$
Density	$\rho_{hnf} = \varphi_2\rho_{s2} + (1-\varphi_2)[(1-\varphi_1)\rho_f + \varphi_1\rho_{s1}]$
Dynamic Viscosity	$\mu_{hnf} = \frac{\mu_f}{(1-\varphi_1)^{2.5}(1-\varphi_2)^{2.5}}$
Thermal Conductivity	$\frac{k_{hnf}}{k_{bf}} = \frac{k_{s2}+2k_{bf}-2\varphi_2(k_{bf}-k_{s2})}{k_{s2}+2k_{bf}+\varphi_2(k_{bf}-k_{s2})}$, $\frac{k_{bf}}{k_f} = \frac{2k_f+k_{s1}-2\varphi_1(k_f-k_{s1})}{2k_f+k_{s1}+\varphi_1(k_f-k_{s1})}$

Given that, φ_1 and φ_2 are hybrid nanofluid volume fraction CuO and hybrid nanofluid volume fraction Ag nanoparticles respectively. Here, f, hnf, $s1$, and $s2$ subscripts represent fluid, hybrid nanofluid, CuO nanoparticle, and Ag nanoparticle, respectively. Then, the following similarity transformation is introduced to reduce the governing equations by Malvadi et al. [33],

$$\eta = \left(\frac{(n+1)b}{2v_f}\right)^{\frac{1}{2}} y\, x^{\frac{n-1}{2}}, \quad \psi = \left(\frac{2bv_f}{n+1}\right)^{\frac{1}{2}} x^{\frac{n+1}{2}} f(\eta), \quad T = (T_w - T_\infty)\theta(\eta) + T_\infty, \tag{5}$$

as η is the independent variable, ψ is the stream function and v_f is the kinematic viscosity. Next, the velocity components can be represented as $v = -\frac{\partial \psi}{\partial x}$ and $u = \frac{\partial \psi}{\partial y}$. By utilizing the defining parameter, Eq. (1) is satisfied and the remaining Eqs. (2)–(3) are changed as follows

$$\frac{\frac{\mu_{hnf}}{\mu_f}}{\frac{\rho_{hnf}}{\rho_f}} f''' + ff'' + \beta(1 - (f')^2) = 0, \tag{6}$$

$$\frac{\frac{k_{hnf}}{k_f}}{\frac{(\rho C_p)_{hnf}}{(\rho C_p)_f}} \cdot \frac{1}{\mathrm{Pr}}\theta'' + \theta' f = 0, \tag{7}$$

transformed boundary conditions

$$\begin{aligned} &f'(0) = \varepsilon + \sigma f''(0), \quad f(0) = 0, \quad \theta(0) = 1 \\ &f'(\eta) \to 1, \quad \theta(\eta), \to 0, \quad \text{as} \ \ \eta \to \infty, \end{aligned} \tag{8}$$

where $\sigma = L_1 x^{-(\frac{n-1}{2})}$ is a velocity slip parameter and prime implies the derivative with respect to η. Then, $\varepsilon = \frac{a}{b}$ can be presented as a stretching/shrinking parameter such that the positive value indicates stretching and the negative value represents shrinking. In addition, Prandtl number is presented by $\mathrm{Pr} = \frac{v}{\alpha}$. Then, the physical quantities required are local skin friction, C_f and shear stress, τ_w,

$$C_f = \frac{\tau_w}{\rho_f U_\infty^2}, \quad \tau_w = \mu_{hnf}(\frac{\partial u}{\partial y})_{y=0}, \tag{9}$$

then the local Nusselt number and heat flux are

$$\mathrm{Nu}_x = \frac{x q_w}{k_f(T_w - T_\infty)}, \quad q_w = -k_{hnf}(\frac{\partial T}{\partial y})_{y=0}. \tag{10}$$

Thus, the above physical quantities are

$$\mathrm{Re}_x^{\frac{1}{2}} C_f = \frac{\mu_{hnf}}{\mu_f}\sqrt{\frac{n+1}{2}} f''(0), \quad \mathrm{Re}_x^{-\frac{1}{2}}\mathrm{Nu}_x = -\frac{k_{hnf}}{k_f}\sqrt{\frac{n+1}{2}}\theta'(0), \tag{11}$$

and $\mathrm{Re}_x = \frac{U_\infty x}{v_f}$ is the local Reynold number.

Numerical solution by Haar wavelet collocation method (HWCM). The semi-infinite physical domain $[0, \infty)$ must be changed to suitable Haar wavelet context where it can be reduced to $[0, 1)$ by introducing the coordinate transformation $\xi = \frac{\eta}{\eta_\infty}$ and changing the variable to $F(\xi) = \frac{f(\eta)}{\eta_\infty}$ and $\theta_1(\xi) = \frac{\theta(\eta)}{\eta_\infty}$ to satisfy all the boundary conditions. Then, Eqs. (6) and (6) can be transformed to

$$\frac{\frac{\mu_{hnf}}{\mu_f}}{\frac{\rho_{hnf}}{\rho_f}} F'''(\xi) + \beta\eta_\infty^2\left(1 - (F'(\xi))^2\right) + \eta_\infty^2 F(\xi)\, F''(\xi) = 0, \tag{12}$$

$$\frac{\frac{k_{hnf}}{k_f}}{\frac{(\rho C_p)_{hnf}}{(\rho C_p)_f}}\frac{1}{\mathrm{Pr}}\,\theta_1''(\xi) + \eta_\infty^2 F(\xi)\,\theta_1'(\xi) = 0. \tag{13}$$

The boundary conditions of (8) are transformed to

$$\begin{gathered} F(0) = 0, \quad \theta_1(0) = \frac{1}{\eta_\infty}, \quad F'(0) = \varepsilon + \sigma F''(0), \\ F'(\eta) \to 1, \quad \theta_1(\eta) \to 0, \quad \text{as} \quad \eta \to \eta_\infty. \end{gathered} \tag{14}$$

The higher order of derivative for (12) and (13) are approximated by Haar wavelet.

$$F'''(\xi) = \sum_{i=1}^{2^{J+1}} a_i h_i(\xi), \tag{15}$$

$$\theta_1''(\xi) = \sum_{i=1}^{2^{J+1}} d_i h_i(\xi). \tag{16}$$

Letting $A = \frac{\eta_\infty}{\sigma+\eta_\infty}$, the corresponding lower order of derivatives are integrated using (15) and (16):

$$F''(\xi) = \sum_{i=1}^{2^{J+1}} a_i P_{1,i}(\xi) + A(1-\varepsilon) - A\sum_{i=1}^{2^{J+1}} a_i C_i, \tag{17}$$

$$F'(\xi) = \sum_{i=1}^{2^{J+1}} a_i\left[P_{2,i}(\xi) - AC_i\left(\xi + \frac{\sigma}{\eta_\infty}\right)\right] + \varepsilon + A(1-\varepsilon)\left(\xi + \frac{\sigma}{\eta_\infty}\right), \tag{18}$$

$$F(\xi) = \sum_{i=1}^{2^{J+1}} a_i\left[P_{3,i}(\xi) - AC_i\left(\frac{\xi^2}{2} + \frac{\xi\sigma}{\eta_\infty}\right)\right] + \xi\varepsilon + A(1-\varepsilon)\left(\frac{\xi^2}{2} + \frac{\xi\sigma}{\eta_\infty}\right), \tag{19}$$

$$\theta_1'(\xi) = \sum_{i=1}^{2^{J+1}} d_i[P_{i,1} - C_i] - \left(\frac{1}{\eta_\infty}\right), \tag{20}$$

$$\theta_1(\xi) = \sum_{i=1}^{2^{J+1}} d_i[P_{i,2} - \xi C_i] - (\xi) + \left(\frac{1}{\eta_\infty}\right). \tag{21}$$

Then, Eqs. (17)–(21) are used in (12) and (13), and by applying the collocation point

$$\xi_l = \frac{1}{2^{J+1}}\left(l - \frac{1}{2}\right), \quad l = 1, 2, \ldots, 2^{J+1}, \tag{22}$$

a numerical solution for the system of nonlinear equations with 2^{J+1} unknown wavelet coefficients can be derived.

4. Result and discussion

The ODEs Eqs. (6) and (7) along with boundary condition equations (8) have been solved and the numerical solutions can be achieved using Maple software for different values of hybrid nanofluid volume fractions φ_1, φ_2, non-linear parameter β, velocity slip parameter σ and stretching/shrinking parameter ε. Consider the values of hybrid nanoparticle volume fractions φ_1,φ_2 in the range from 0 to 0.2 and Pr is 6.2 for base fluid which is defined as water. While the value of the nonlinear parameter β varies from 1 to 2. The value of the velocity slip parameter ε is in the range from 0 to 0.4. The basic properties of nanoparticles and base fluid are shown in Table 2 [34]. The present results of $f''(0)$ and $-\theta'(0)$ have been validated with past studies results by Anuar et al. [35] as in Table 3.

Table 2. Thermophysical properties of nanoparticle.

Properties	CuO	Ag	Base fluid (water)
ρ (kg m^{-3})	10500	6320	997.1
k (W m^{-1}K^{-1})	429	76.50	0.613
C_p (J kg^{-1}K^{-1})	235	531.80	4179

Table 3. $f''(0)$ and $-\theta'(0)$ when $\varphi_1 = \varphi_2 = 0$, $\beta = 1$, Pr $= 0.7$ and $\varepsilon = -1.1$.

Anuar et al.		Current result	
$f''(0)$	$-\theta'(0)$	$f''(0)$	$-\theta'(0)$
1.18668	0.18283	1.187447570	0.1828396902
[0.04923]	[0.00008]	[0.04923004613]	[0.0000801526]

"[ ]" second solution

Figures 2 and 3 show the impact of Ag nanoparticle φ_2 on the velocity profile $f'(\eta)$ and temperature profile $\theta(\eta)$ for the shrinking case along with $\sigma = 0.2$ and $\beta = \frac{4}{3}$. It is found that $f'(\eta)$ escalates within the momentum boundary layer due to the increasing value of φ_2 for the first and second solutions. Meanwhile, $\theta(\eta)$ reduces with the increasing value of φ_2 for both solutions. Consequently, it causes the thinning of the boundary layer thickness. Thus, duality exists for $\varepsilon = -1.2$. Figures 3 and 4 present the results of skin friction $f''(0)$ and heat transfer $-\theta'(0)$ graphs for certain values of stretching/shrinking parameter ε for diverse values of hybrid nanofluid volume fraction φ_2 with $\varphi_1 = 0.1$, $\sigma = 0.2$ and $\beta = \frac{4}{3}$. It is noticed that duality exists when $\varepsilon \leqslant -1$ and also unique solutions were obtained when $\varepsilon > -1$, but there is no solution when $\varepsilon < \varepsilon_c$ due to the boundary layer separations are bound to occur and the boundary layer approximation cannot be done further this critical values ε_c. Moreover, the significance of $f''(0)$ is raised with the increasing values of φ_2. Whereas, the increasing values of φ_2 causing the reducing values of $-\theta'(0)$ when $\varepsilon > -0.5$ and the inverse pattern are discovered when $\varepsilon < -0.5$. Hence, lowering the momentum boundary layer thickness causes an increasing in skin friction and enhanced heat conduction at the surface.

Figures 6 and 7 display the effect of various velocity slip σ values on $f'(\eta)$ and $\theta(\eta)$ for shrinking case ($\varepsilon < -1$) with $\varphi_1 = \varphi_2 = 0.1$, $\varepsilon = -1.2$ and $\beta = \frac{4}{3}$. From both figures, $f'(\eta)$ increases in the momentum boundary layer for the first solution but decreases for the second solution. But contrary result is for $\theta(\eta)$ where it decreases in thermal boundary layer for the first solution but it increases for the second solution. Figures 8 and 9 show the $f''(0)$ and $-\theta'(0)$ graphs for certain values of ε and

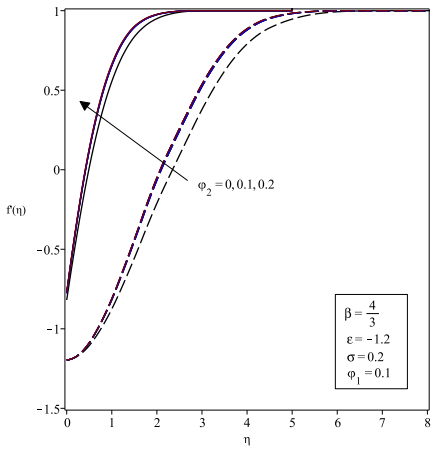

Fig. 2. Velocity profile with σ for different φ_2.

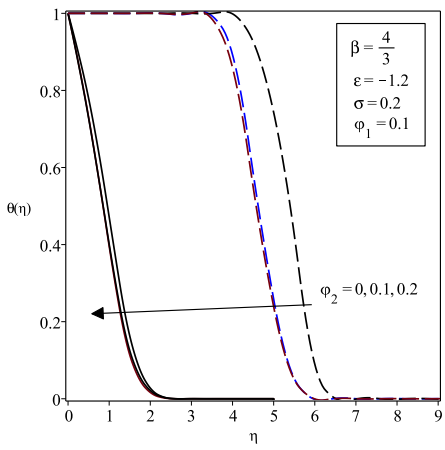

Fig. 3. Temperature profile with σ for different φ_2.

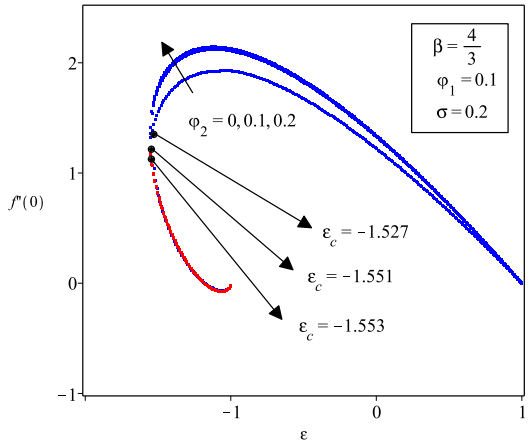

Fig. 4. $f''(0)$ with ε for different φ_2.

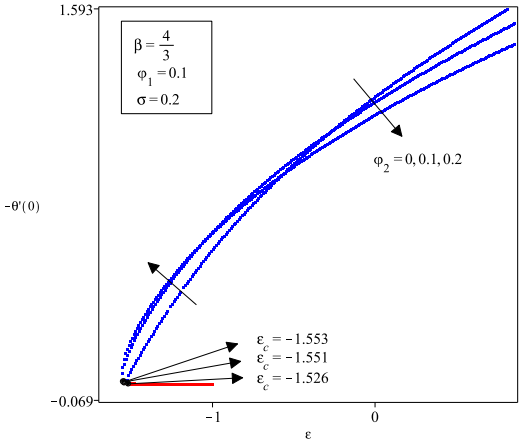

Fig. 5. $-\theta(0)$ with ε for different φ_2.

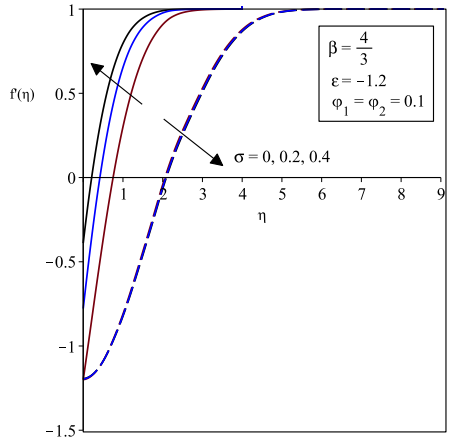

Fig. 6. Velocity profile for different σ.

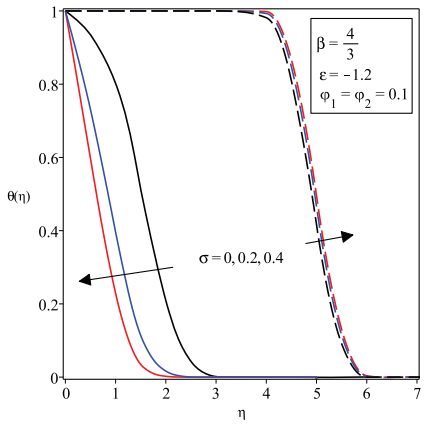

Fig. 7. Temperature profile for different σ.

various values of velocity slip parameter σ for hybrid nanofluids with $\varphi_1 = \varphi_2 = 0.1$ and $\beta = \frac{4}{3}$. Both graphs show the range of ε for $(\varepsilon \geqslant \varepsilon_c)$ indicate the existence of dual solutions when the value of σ increased at the boundary. For both figures, as σ is increasing, the range of similarity solutions is increasing. The same conclusion is for the existence of duality in both figures and there is no solution whenever the values of $(\varepsilon < \varepsilon_c)$. This shows that the larger value of σ delays the separation of boundary layers because the fluid can continue to move more rapidly near the surface, resisting separation. The second solution has a lesser magnitude of $f''(0)$ and $-\theta'(0)$ as given ε rather than the first solution.

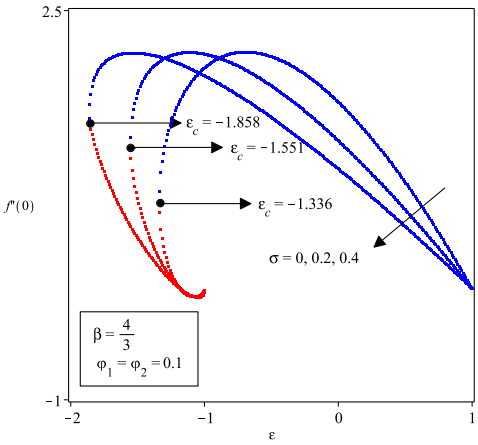

Fig. 8. $f''(0)$ with ε for different σ.

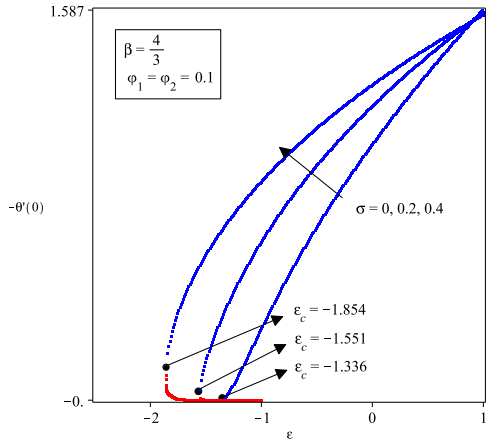

Fig. 9. $-\theta'(0)$ with ε for different σ.

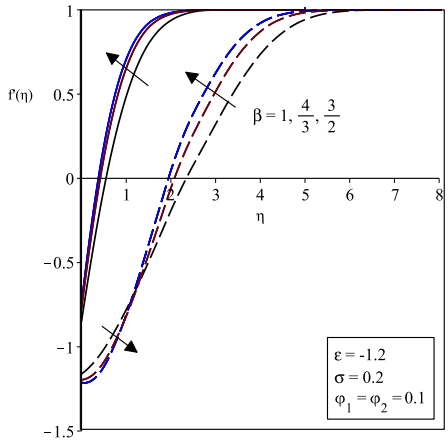

Fig. 10. Velocity profile with σ for different β.

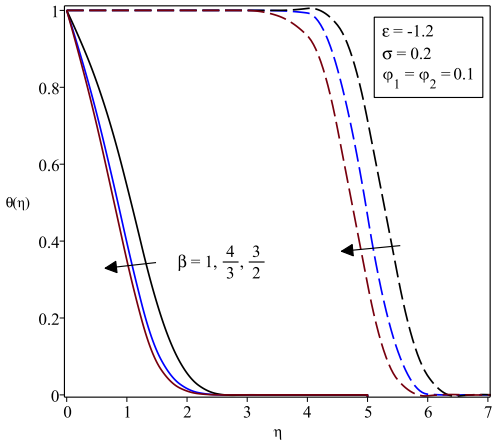

Fig. 11. Temperature profile with σ for different β.

Figures 10 and 11 demonstrate the outcome of different nonlinear parameter β on the dimensionless velocity $f'(\eta)$ and temperature $\theta(\eta)$ for a shrinking case which is $\varepsilon = -1.2$ using $\varphi_1 = \varphi_2 = 0.1$ with $\sigma = 0.2$. Dual solutions are obtained in both velocity and temperature profiles. From Figure 10, it is noted that as β grows, $f'(\eta)$ rises in the momentum boundary layer for the first and second solutions. Nevertheless, $\theta(\eta)$ reduces in the thermal boundary layer for both solutions as β increases. Figures 12 and 13 demonstrate the results of different values of nonlinear parameter on $f''(0)$ and $-\theta'(0)$ for certain values of ε when $\varphi_1 = \varphi_2 = 0.1$ with the presence of $\sigma = 0.2$. For both figures, as β is increasing, the range of similarity solutions is increasing. The same conclusion is made for the existence of duality in both figures and there is no solution whenever the values of $(\varepsilon < \varepsilon_c)$. This indicates that the larger value of β delays the separation of the boundary layer. The second solution has a lesser magnitude of $f''(0)$ and $-\theta'(0)$ as provided ε rather than the first solution. Thus, $f''(0)$ and $-\theta'(0)$ increase due to the growing nonlinear parameter β.

Figures 14 and 15 illustrate the variations of $\mathrm{Re}_x^{\frac{1}{2}} C_f$ and $\mathrm{Re}_x^{\frac{-1}{2}} \mathrm{Nu}_x$ which are local skin friction and local Nusselt respectively for various values of nanoparticle volume fraction φ_1 and φ_2 with different σ for $\varepsilon = 0.5$ and $\beta = \frac{4}{3}$. It is noticed that the skin friction coefficient decreases when the value of σ increased. Unlike local Nusselt, it increases as the value of σ increases therefore enhance the heat transfer rate. Figures 16 and 17 show the value of $\mathrm{Re}_x^{\frac{1}{2}} C_f$ and $\mathrm{Re}_x^{\frac{-1}{2}} \mathrm{Nu}_x$ with $\varepsilon = 0.5$, and $\sigma = 0.2$ for different value of β. It can be found that by making use of various values of hybrid nanofluid volume fractions (φ_1, φ_2) impact a change in local skin friction and Nusselt number. As the value β becomes greater, the value for both $\mathrm{Re}_x^{\frac{1}{2}} C_f$ and $\mathrm{Re}_x^{\frac{-1}{2}} \mathrm{Nu}_x$ increase as well.

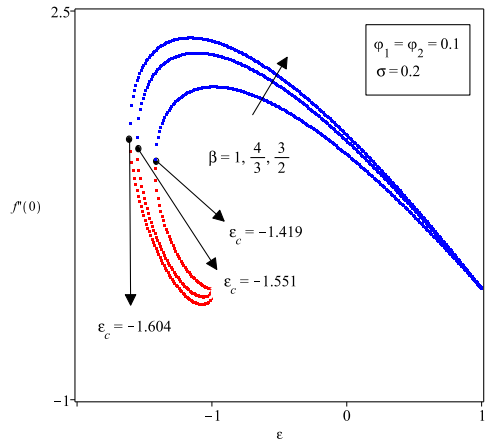

Fig. 12. $f''(0)$ with ε for different β.

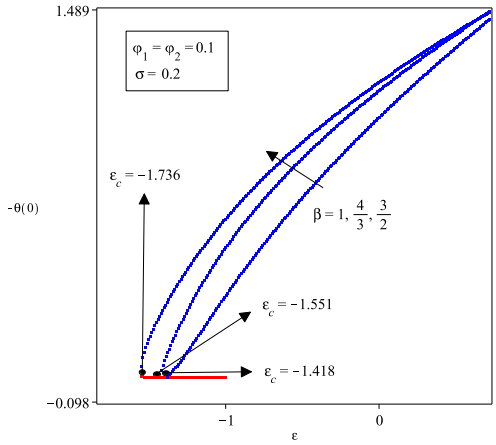

Fig. 13. $-\theta'(0)$ with ε for different β.

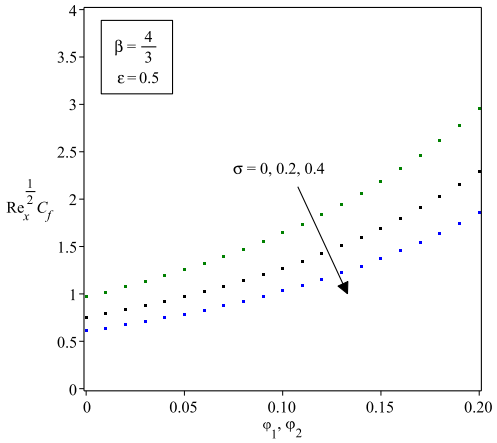

Fig. 14. Local skin friction coefficient for different σ.

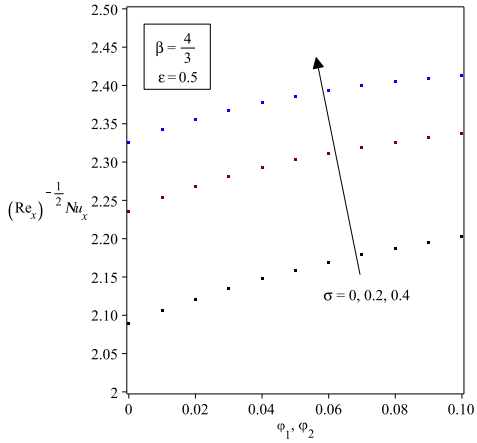

Fig. 15. Local Nusselt number for different σ.

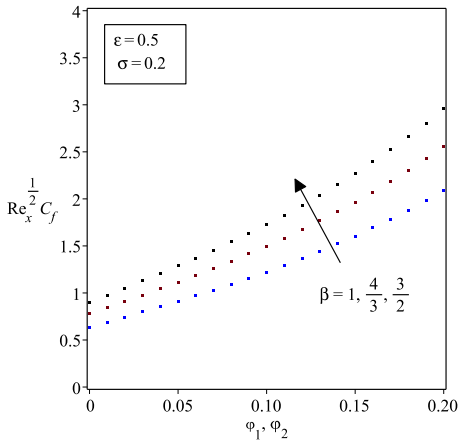

Fig. 16. Local skin friction coefficient for different β.

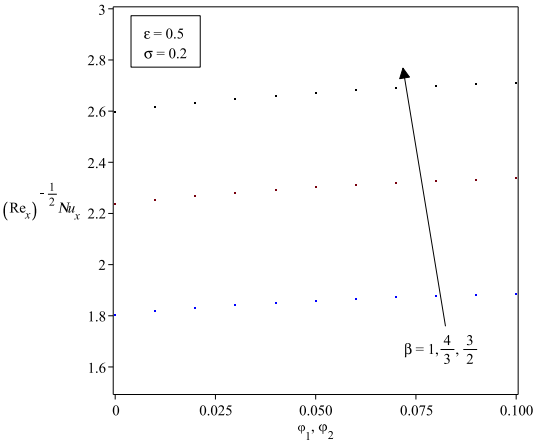

Fig. 17. Local Nusselt number for different β.

Figures 18 and 19 portray the response of viscous flow (i.e. $\varphi_1 = \varphi_2 = 0$), CuO/water nanofluid (i.e. $\varphi_1 = 0.1$, $\varphi_2 = 0$) and Ag-CuO/water hybrid nanofluid (i.e. $\varphi_1 = \varphi_2 = 0.1$) with $\beta = \frac{4}{3}$, $\sigma = 0.2$ and $\varepsilon = -1.2$. As the value of φ_1 and φ_2 rising, the magnitude of $f'(\eta)$ increases, meanwhile $\theta(\eta)$ decreases. Therefore, the momentum and thermal boundary layer thicknesses of hybrid nanofluid are thinner than nanofluid, implying that hybrid nanofluid has a higher skin friction and heat transfer rate than nanofluid.

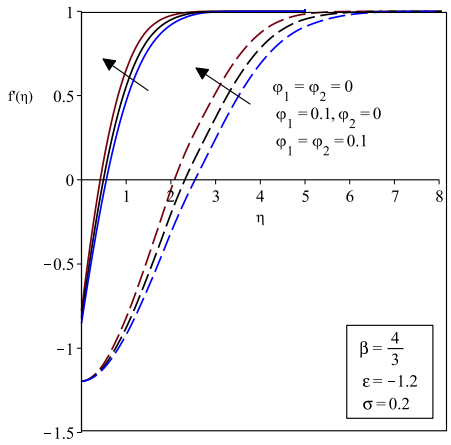

Fig. 18. Velocity profile with σ for different φ.

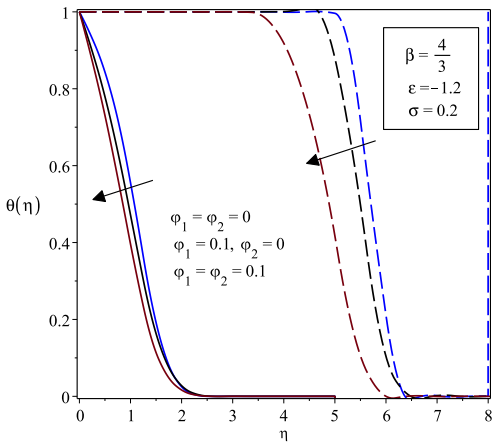

Fig. 19. Temperature profile with σ for different φ.

5. Conclusion

The problem of stagnation point flow over a nonlinearly stretching/shrinking surface in hybrid nanofluid with slip effects was studied numerically. The consideration of the parameters such as hybrid nanofluid volume fractions φ_1, φ_2, non-linear parameter β, velocity slip parameter σ and stretching/shrinking parameter ε were solved using numerical technique based on Haar wavelets collocation.

— It can be found where the shrinking sheet gives dual solutions at a certain limit and the stretching sheet gives unique solutions.
— The increasing of the nonlinear parameter β and velocity slip parameter σ postpone the boundary layer separation as both parameters widen the range of solutions.
— As nanoparticle volume fraction φ_2 and β increase in shrinking case, both increase the velocity profile, but reduce the temperature profile for both solutions.
— When the velocity slip parameter σ increases, it increases the velocity profile for the first solution and decreases for the second solution. It also decreases the temperature profile for the first solution but increases for the second solution.
— Local skin friction coefficient and local Nusselt number can be intensified by the addition of nonlinear parameter β and nanoparticle volume fraction φ_1, φ_2. Different results are obtained when σ and nanoparticle volume fraction φ_1, φ_2 increase, Nusselt number increases but local skin friction decreases.

[1] Choi S. U. S., Eastman J. A. Enhancing thermal conductivity of fluids with nanoparticles. Argonne National Lab.(ANL), Argonne, IL (United States) (1995).

[2] Li J., Zhang X., Xu B., Yuan M. Nanofluid research and applications: A review. International Communications in Heat and Mass Transfer. **127**, 105543 (2021).

[3] Lenin R., Joy P. A., Bera C. A review of the recent progress on thermal conductivity of nanofluid. Journal of Molecular Liquids. **338**, 116929 (2021).

[4] Esfe M. H., Afrand M., Karimipour A., Yan W.-M., Sina N. An experimental study on thermal conductivity of MgO nanoparticles suspended in a binary mixture of water and ethylene glycol. International Communications in Heat and Mass Transfer. **67**, 173–175 (2015).

[5] Suresh S., Venkitaraj K. P., Selvakumar P., Chandrasekar M. Synthesis of Al_2O_3-Cu/water hybrid nanofluids using two step method and its thermo physical properties. Colloids and Surfaces A: Physicochemical and Engineering Aspects. **388** (1–3), 41–48 (2011).

[6] Momin G. G. Experimental investigation of mixed convection with water-Al_2O_3 and hybrid nanofluid in inclined tube for laminar flow. International Journal of Scientific & Technology Research. **2** (12), 195–202 (2013).

[7] Huminic G., Huminic A. Hybrid nanofluids for heat transfer applications – A state-of-the-art review. International Journal of Heat and Mass Transfer. **125**, 82–103 (2018).

[8] Muneeshwaran M., Srinivasan G., Muthukumar P., Wang C.-C. Role of hybrid-nanofluid in heat transfer enhancement – A review. International Communications in Heat and Mass Transfer. **125**, 105341 (2021).

[9] Vallejo J. P., Prado J. I., Lugo L. Hybrid or mono nanofluids for convective heat transfer applications. A critical review of experimental research. Applied Thermal Engineering. **203**, 117926 (2022).

[10] Devi Uma S. S., Devi S. A. Numerical investigation of three-dimensional hybrid Cu-Al_2O_3/water nanofluid flow over a stretching sheet with effecting Lorentz force subject to Newtonian heating. Canadian Journal of Physics. **94** (5), 490–496 (2016).

[11] Hayat T., Nadeem S. Heat transfer enhancement with Ag-CuO/water hybrid nanofluid. Results in Physics. **7**, 2317–2324 (2017).

[12] Anuar N. S, Bachok N., Pop I. Influence of MHD hybrid ferrofluid flow on exponentially stretching/shrinking surface with heat source/sink under stagnation point region. Mathematics. **9** (22), 2932 (2021).

[13] Aly E. H., Pop I. MHD flow and heat transfer over a permeable stretching/shrinking sheet in a hybrid nanofluid with a convective boundary condition. International Journal of Numerical Methods for Heat & Fluid Flow. **29** (9), 3012–3038 (2019).

[14] Khashi'ie N. S., Wahi N., Arifin N. M., Ghani A. A., Hamzah K. B. Effect of suction on the MHD flow in a doubly-stratified micropolar fluid over a shrinking sheet. Mathematical Modeling and Computing. **9** (1), 92–100 (2022).

[15] Alias N. S., Hafidzuddin M. E. H. Effect of suction and MHD induced Navier slip flow due to a non-linear stretching/shrinking sheet. Mathematical Modeling and Computing. **9** (1), 83–91 (2022).

[16] Lee J., Kim D. H. An improved shooting method for computation of effectiveness factors in porous catalysts. Chemical Engineering Science. **60** (20), 5569–5573 (2005).

[17] Michalik C., Hannemann R., Marquardt W. Incremental single shooting – A robust method for the estimation of parameters in dynamical systems. Computers & Chemical Engineering. **33** (7), 1298–1305 (2009).

[18] Karkera H., Katagi N. N., Kudenatti R. B. Analysis of general unified MHD boundary-layer flow of a viscous fluid – a novel numerical approach through wavelets. Mathematics and Computers in Simulation. **168**, 135–154 (2020).

[19] Daubechies I. Ten Lectures on Wavelets. Society for Industrial and Applied Mathematics (1992).

[20] Chen C. F., Hsiao C. H. Haar wavelet method for solving lumped and distributed-parameter systems. IEE Proceedings – Control Theory and Applications. **144** (1), 87–94 (1997).

[21] Lepik Ü. Numerical solution of differential equations using Haar wavelets. Mathematics and Computers in Simulation. **68** (2), 127–143 (2005).

[22] Sathar M. H. A., Rasedee A. F. N., Ahmedov A. A., Bachok N. Numerical solution of nonlinear Fredholm and Volterra integrals by Newton–Kantorovich and Haar wavelets methods. Symmetry. **12** (12), 2034 (2020).

[23] Aziz I., Amin R. Numerical solution of a class of delay differential and delay partial differential equations via Haar wavelet. Applied Mathematical Modelling. **40** (23–24), 10286–10299 (2016).

[24] Ahmedov A. A., Sathar M. H. A., Rasedee A. F. N., Mokhtar N. F. B. Approximating of functions from Holder classes $H^{\alpha}[0,1]$ by Haar wavelets. Journal of Physics: Conference Series. **890** (1), 012073 (2017).

[25] Saeed U., Rehman M. U. Wavelet–Galerkin quasilinearization method for nonlinear boundary value problems. Abstract and Applied Analysis. **2014**, 868934 (2014).

[26] Arifeen S. U., Haq S., Ghafoor A., Ullah A., Kumam P., Chaipanya P. Numerical solutions of higher order boundary value problems via wavelet approach. Advances in Difference Equations. **2021**, 347 (2021).

[27] Katagi N., Karkera H., Kudenatti R. Analysis of laminar boundary–layer flow over a moving wedge using a uniform haar wavelet method. Frontiers in Heat and Mass Transfer (FHMT). **18**, 41 (2022).

[28] Bachok N., Ishak A., Nazar R., Senu N. Stagnation-point flow over a permeable stretching/shrinking sheet in a copper-water nanofluid. Boundary Value Problems. **2013**, 39 (2013).

[29] Anuar N. S., Bachok N., Arifin N. M., Rosali H. Role of multiple solutions in flow of nanofluids with carbon nanotubes over a vertical permeable moving plate. Alexandria Engineering Journal. **59** (2), 763–773 (2020).

[30] Subhani M., Nadeem S. Numerical analysis of micropolar hybrid nanofluid. Applied Nanoscience. **9**, 447–459 (2019).

[31] Tayebi T., Chamkha A. J. Entropy generation analysis during MHD natural convection flow of hybrid nanofluid in a square cavity containing a corrugated conducting block. International Journal of Numerical Methods For Heat & Fluid Flow. **30** (3), 1115–1136 (2019).

[32] Ranga Babu J. A., Kumar K. K., Rao S. S. State-of-art review on hybrid nanofluids. Renewable and Sustainable Energy Reviews. **77**, 551–565 (2017).

[33] Malvandi A., Hedayati F., Ganji D. D. Nanofluid flow on the stagnation point of a permeable non-linearly stretching/shrinking sheet. Alexandria Engineering Journal. **57** (4), 2199–2208 (2018).

[34] Oztop H., Abu-Nada E. Numerical study of natural convection in partially heated rectangular enclosures filled with nanofluids. International Journal of Heat and Fluid Flow. **29** (5), 1326–1336 (2008).

[35] Anuar N. S., Bachok N., Arifin N. M., Rosali H. Numerical solution of stagnation point flow and heat transfer over a nonlinear stretching/shrinking sheet in hybrid nanofluid: Stability analysis. Journal of Advanced Research in Fluid Mechanics and Thermal Sciences. **76** (2), 85–98 (2020).

Метод вейвлет-колокації Хаара для розв'язування точки застою над листом, що нелінійно розтягується/стискається, у гібридній нанорідині з ефектом ковзання

Хасана Н. С.[1], Раседі А. Ф. Н.[2], Бачок Н.[1], Вонг Т. Ж.[3], Хасан М.[4]

[1] *Кафедра математики та статистики, факультет природничих наук, Університет Путра Малайзії, 43400 Серданг, Селангор, Малайзія*
[2] *Факультет економіки і муамалата, Університет Саінс Ісламу Малайзія, Малайзія*
[3] *Кафедра фундаментальних наук та техніки, факультет сільського господарства та харчових наук, Університет Путра Малайзія, кампус Бінтулу, Ньябау Роуд, Бінтулу, Саравак, 97008, Малайзія*
[4] *Центр фундаментальних досліджень сільськогосподарської науки, Університет Путра Малайзії*

Дослідження потоку в точці застою та теплопередачі через лист, що розтягується/стискається, у гібридній нанофлюїді має потенційне застосування в різних галузях. Щоб дослідити властивості течії рідини та теплообміну, необхідно розв'язати основну математичну модель (рівняння в частинних похідних). Використовуючи змінні подібності, модель перетворюється на систему звичайних диференціальних рівнянь. Використовується нова чисельна схема, яка поєднує потужність вейвлетів Хаара з методом колокації для розв'язування цих звичайних диференціальних рівнянь. Завдяки цьому підходу можна передбачити декілька важливих величин, пов'язаних із потоком рідини та теплопередачею, включаючи коефіцієнт поверхневого тертя, локальне число Нуссельта, а також профілі швидкості та температури, на які можуть впливати основні параметри моделі.

Ключові слова: *гібридні нанорідини; нелінійне розтягування/стиснення; точка застою; вейвлет Хаара.*